

# Structural Aspects of the Dehydration and Dehydroxylation of $\gamma$ -Titanium Phosphate, $\gamma$ -Ti(PO<sub>4</sub>)(H<sub>2</sub>PO<sub>4</sub>)·2H<sub>2</sub>O

Anne Marie Krogh Andersen\*

Chemistry Department, University of Odense, 5230 Odense M, Denmark

Poul Norby†

Department of Chemistry, SUNY at Stony Brook, Stony Brook, New York 11794

Received February 19, 1998

The thermal transformations of  $\gamma$ -titanium phosphate,  $\gamma$ -Ti(PO<sub>4</sub>)(H<sub>2</sub>PO<sub>4</sub>)·2H<sub>2</sub>O, have been studied using thermogravimetric analysis, differential scanning calorimetry, X-ray powder diffraction, and temperature-resolved in-situ powder diffraction. The transformation sequence goes from  $\gamma$ -Ti(PO<sub>4</sub>)(H<sub>2</sub>PO<sub>4</sub>)·2H<sub>2</sub>O over a new partially dehydrated form  $\gamma'$ -Ti(PO<sub>4</sub>)(H<sub>2</sub>PO<sub>4</sub>)·(2- $x$ )H<sub>2</sub>O ( $x \sim 1$ ) to the anhydrous form  $\beta$ -Ti(PO<sub>4</sub>)(H<sub>2</sub>PO<sub>4</sub>) and then through a two-step condensation process where layered titanium pyrophosphate, Ti(PO<sub>4</sub>)(H<sub>2</sub>P<sub>2</sub>O<sub>7</sub>)<sub>0.5</sub>, is formed first and finally cubic titanium pyrophosphate TiP<sub>2</sub>O<sub>7</sub>. The dehydration of  $\gamma$ -Ti(PO<sub>4</sub>)(H<sub>2</sub>PO<sub>4</sub>)·2H<sub>2</sub>O and the dehydroxylation/condensation process from  $\beta$ -Ti(PO<sub>4</sub>)(H<sub>2</sub>PO<sub>4</sub>) to layered titanium pyrophosphate, Ti(PO<sub>4</sub>)(H<sub>2</sub>P<sub>2</sub>O<sub>7</sub>)<sub>0.5</sub>, was followed in-situ. A new partially dehydrated phase,  $\gamma'$ -Ti(PO<sub>4</sub>)(H<sub>2</sub>PO<sub>4</sub>)·(2- $x$ )H<sub>2</sub>O ( $x \sim 1$ ), which forms at approximately 50 °C has been detected and characterized. The unit cell is monoclinic with the lattice parameters  $a = 23.670(1)$  Å,  $b = 6.264(1)$  Å,  $c = 5.036(1)$  Å,  $\beta = 102.41(1)^\circ$ , and  $Z = 4$ . Layered titanium pyrophosphate, Ti(PO<sub>4</sub>)(H<sub>2</sub>P<sub>2</sub>O<sub>7</sub>)<sub>0.5</sub>, which forms at 375 °C has been characterized. The unit cell is monoclinic with lattice parameters  $a = 16.271(3)$  Å,  $b = 6.319(1)$  Å,  $c = 5.122(1)$  Å,  $\beta = 90.59(2)^\circ$ , and  $Z = 4$ .

## Introduction

Two different types of layered titanium phosphates have earlier been characterized chemically and crystallographically:  $\alpha$ -Ti(HPO<sub>4</sub>)<sub>2</sub>·H<sub>2</sub>O ( $\alpha$ -TiP) and  $\gamma$ -Ti(PO<sub>4</sub>)(H<sub>2</sub>PO<sub>4</sub>)·2H<sub>2</sub>O ( $\gamma$ -TiP).  $\alpha$ -TiP has recently been shown to be isostructural with  $\alpha$ -ZrP.<sup>1</sup> The structure of  $\alpha$ -Zr(HPO<sub>4</sub>)<sub>2</sub>·H<sub>2</sub>O ( $\alpha$ -ZrP) was solved by single-crystal methods by Clearfield *et al.*<sup>2</sup> in 1969. The existence of the  $\gamma$ -layered compounds was first reported in 1968 by Clearfield *et al.*,<sup>3</sup> who prepared Zr(PO<sub>4</sub>)(H<sub>2</sub>PO<sub>4</sub>)·2H<sub>2</sub>O and Zr(PO<sub>4</sub>)(H<sub>2</sub>PO<sub>4</sub>). The prefix  $\gamma$  was assigned to the dihydrate and the prefix  $\beta$  to the anhydrous compound. The formula was originally given as  $\gamma$ -Zr(HPO<sub>4</sub>)<sub>2</sub>·2H<sub>2</sub>O. However, <sup>31</sup>P MAS NMR studies performed by Clayden<sup>4</sup> showed that  $\gamma$ -ZrP contains tertiary phosphate groups and dihydrogen phosphate groups in equal amounts while  $\alpha$ -ZrP only contains monohydrogen phosphate groups. In 1990 Christensen *et al.*<sup>5</sup> proposed a structure for  $\gamma$ -TiP from powder diffraction data that was in accordance with the results of Clayden. In 1995 the structure of  $\gamma$ -ZrP was solved from X-ray powder diffraction data by Poojary *et al.*<sup>6</sup> Recently a structure determination of the

$\beta$ -titanium phosphate<sup>7</sup> showed that the structure of the  $\gamma$ -type layer is retained in the anhydrous compound.

The structure of  $\gamma$ -zirconium phosphate consists of ZrO<sub>6</sub> octahedra linked together by tertiary phosphate tetrahedra (PO<sub>4</sub>) and dihydrogen phosphate tetrahedra (PO<sub>2</sub>(OH)<sub>2</sub>). The PO<sub>4</sub> tetrahedra are sandwiched between two layers of ZrO<sub>6</sub> octahedra, so that all four oxygen atoms bind to zirconium atoms. In the dihydrogen phosphate groups, two oxygen atoms bind to zirconium atoms and the two remaining oxygen atoms form OH groups which point toward the interlayer space. The water molecules reside in pockets which are formed by the hydroxyl groups.<sup>6</sup>

The aim of the present work is to study in detail the dehydration and dehydroxylation of  $\gamma$ -Ti(PO<sub>4</sub>)(H<sub>2</sub>PO<sub>4</sub>)·2H<sub>2</sub>O ( $\gamma$ -TiP) and to characterize the phases that are obtained when  $\gamma$ -titanium phosphate is heated. A new partially dehydrated phase,  $\gamma'$ -Ti(PO<sub>4</sub>)(H<sub>2</sub>PO<sub>4</sub>)·(2- $x$ )H<sub>2</sub>O ( $x \sim 1$ ), has been detected and characterized using thermogravimetric analysis, differential scanning calorimetry, temperature-resolved in-situ synchrotron powder diffraction, and X-ray powder diffraction. Furthermore the layered pyrophosphate phase which is obtained after the first dehydroxylation step has been characterized using X-ray powder diffraction.

## Experimental Section

**Preparation.** The chemicals used in the preparation of  $\gamma$ -titanium phosphate were TiCl<sub>4</sub> (Aldrich), orthophosphoric acid (Fluka, 85%), and hydrochloric acid.

(7) Krogh Andersen, A. M.; Norby, P.; Vogt, T. J. *Solid State Chem.*, accepted.

\* To whom correspondence should be addressed.

† Present address: Chemistry Department, University of Aarhus, 8000 Aarhus C, Denmark.

(1) Bruque, S.; Aranda, M. A. G.; Losilla, E. R.; Olivera-Pastor, P.; Maireles-Torres, P. *Inorg. Chem.* **1995**, *34*, 893.

(2) Clearfield, A.; Smith, G. D. *Inorg. Chem.* **1969**, *8*, 431.

(3) Clearfield, A.; Blessing, R. H.; Stynes, J. A. J. *Inorg. Nucl. Chem.* **1968**, *30*, 249.

(4) Clayden, N. J. *J. Chem. Soc., Dalton Trans.* **1987**, 1877.

(5) Christensen, A. N.; Andersen, E. K.; Andersen, I. G. K.; Alberti, G.; Nielsen, M.; Lehmann, M. S. *Acta Chem. Scand.* **1990**, *44*, 865.

(6) Poojary, D. M.; Shpeizer, B.; Clearfield, A. J. *J. Chem. Soc., Dalton Trans.* **1995**, 111.

Crystalline  $\gamma$ -titanium phosphate was prepared by hydrothermal treatment of amorphous titanium phosphate.<sup>7</sup> The amorphous titanium phosphate, prepared as described by Alberti et al.,<sup>8</sup> was placed in a Teflon-lined autoclave, and phosphoric acid (85%) was added. After stirring for 24 h the autoclave was sealed and heated in an oven at 225 °C for 48 h. After quenching the solid was isolated by filtration, washed with water and air-dried. The product was pure and crystalline  $\gamma$ -TiP.

Samples for examination of the unit cell parameters versus temperature, were prepared by heating  $\gamma$ -titanium phosphate in a platinum crucible for 24 h at temperatures between 200 and 1000 °C.

**Characterization.** Temperature-resolved in-situ synchrotron powder diffraction experiments were performed at the beamline X7B at the National Synchrotron Light Source (NSLS) at Brookhaven National Laboratory (BNL). The low-temperature data were collected from 4 to 112° in  $2\theta$  using an INEL CP120 position sensitive detector. The wavelength used was 1.4898 Å. The samples, which were contained in quartz capillaries, were heated at a rate of 2.5 °C/min from room temperature to 98 °C. The high-temperature data were recorded using the translating imaging plate (TIP)<sup>9</sup> camera which has been built especially for time- and temperature-dependent experiments. The wavelength was 0.9364 Å. The samples were contained in 0.5 mm quartz capillaries and heated to 930 °C using an Enraf-Nonius heatergun. The heating rate was 7.5 °C/min.

X-ray powder patterns were obtained using a Siemens D5000 diffractometer equipped with a primary germanium monochromator (Cu K $\alpha_1$  radiation,  $\lambda = 1.540598$  Å). The data were recorded using reflection geometry from 2 to 90° in  $2\theta$  using a step length of 0.02° and a counting time of 15 s per step. The trial-and-error indexing program TREOR<sup>10</sup> was used to determine unit cell parameters for the various phases. The program CELLKANT<sup>11</sup> was used to refine the unit cell parameters from the observed  $d$  spacings. The Figure of Merit<sup>12</sup> (M(20)) for the various phases is given in the tables.

Infrared spectra were recorded using a Perkin-Elmer Fourier transform IR spectrometer 170. The KBr pellet technique was used. The spectral resolution was 2 cm<sup>-1</sup>.

Thermogravimetric analysis was performed using a Setaram TG92-12 instrument. The heating rate was 5 °C/min and the experiments were performed in nitrogen flow.

Differential scanning calorimetry (DSC) was performed using a Setaram DTA92-16.18 instrument. The samples were placed in a platinum crucible, and  $\alpha$ -Al<sub>2</sub>O<sub>3</sub> was used as reference. Heating and cooling rates of 5 and 10 °C/min were used. The experiments were performed in argon atmosphere. The temperature and enthalpy change calibration was carried out using the low-high quartz transition and the dehydration of gypsum, CaSO<sub>4</sub>·2H<sub>2</sub>O.

## Results and Discussion

**$\gamma'$ -Titanium Phosphate.** Figure 1 shows the TG and DSC curve for  $\gamma$ -Ti(P<sub>2</sub>O<sub>7</sub>)(H<sub>2</sub>PO<sub>4</sub>)·2H<sub>2</sub>O ( $\gamma$ -TiP) in the temperature range 25–250 °C. It can be seen from the TG curve that the compound loses two moles of crystal water in the range from 50 to 100 °C. This leads to the formation of the anhydrous form  $\beta$ -Ti(P<sub>2</sub>O<sub>7</sub>)(H<sub>2</sub>PO<sub>4</sub>) ( $\beta$ -TiP). This dehydration has been described by several authors.<sup>13–15</sup> However, only La Ginestra and Massucci<sup>15</sup> describe a two-step transformation with the formation of an intermediate phase. From the DSC curve in Figure 1 it is clearly seen that the dehydration takes place in two steps. This observation is supported by in-situ temperature-

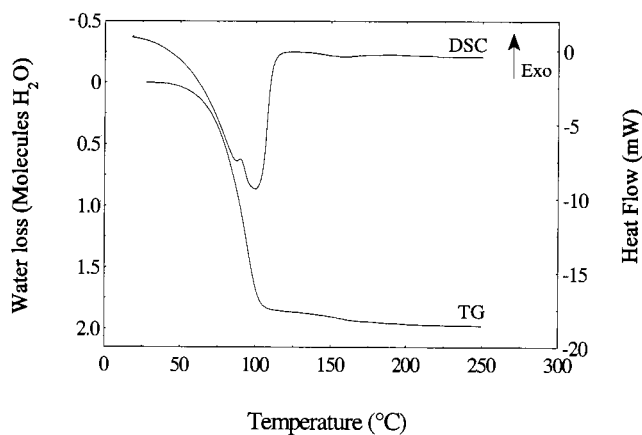
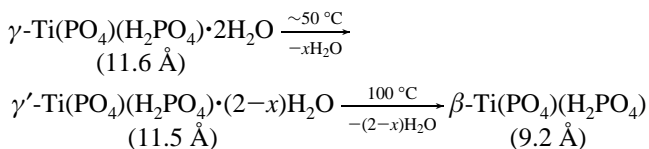


**Figure 1.** TG and DSC curve for  $\gamma$ -Ti(P<sub>2</sub>O<sub>7</sub>)(H<sub>2</sub>PO<sub>4</sub>)·2H<sub>2</sub>O in the temperature range 25–250 °C.

resolved synchrotron data and X-ray powder diffraction data which show that an intermediate phase is formed between  $\gamma$ -TiP and  $\beta$ -TiP. The new phase, in the following called  $\gamma'$ -TiP, contains ~1 mol of crystal water. This two-step process can be summarized as follows (the interlayer distances are given in parentheses):



$\gamma'$ -TiP was first detected in a series of temperature-resolved in-situ synchrotron powder patterns (Figure 2). The patterns were recorded at the National Synchrotron Light Source (NSLS) at Brookhaven National Laboratory (BNL). The temperature range is 38–98 °C.  $\gamma'$ -TiP only exists in a very narrow temperature interval from 60 to 80 °C. Only in the highlighted pattern in Figure 2 was  $\gamma'$ -TiP found as the pure phase.

To obtain an X-ray powder pattern of the pure phase of  $\gamma'$ -TiP, for further structural investigation, a heating device was constructed which could be used while recording the pattern on the diffractometer. It was found that the pure phase could be obtained by heating  $\gamma$ -TiP to 54 °C and then lowering the temperature to 40 °C. This way it was possible to keep the pure phase for 24 h, which was sufficient time to record a good pattern. If the temperature was not lowered  $\gamma'$ -TiP was slowly converted into  $\beta$ -TiP. The indexed X-ray powder pattern of  $\gamma'$ -TiP is provided in Table 1. The unit cell dimensions are:  $a = 23.670(3)$  Å,  $b = 6.264(1)$  Å,  $c = 5.036(1)$  Å, and  $\beta = 102.41(1)^\circ$ . For comparison it should be mentioned that the unit cell of  $\gamma$ -TiP is  $a = 23.742(1)$  Å,  $b = 6.346(1)$  Å,  $c = 5.179(1)$  Å, and  $\beta = 102.54(1)^\circ$ . A possible space group for  $\gamma'$ -TiP is  $P2_1(0k0)$  ( $k = 2n + 1$ ) being the only systematic extinction). Profile fitting with ALLHKL<sup>16</sup> confirms this space group.

To obtain information about the structural changes that take place during the formation of  $\gamma'$ -TiP, the temperature dependence of the unit cell volume and the lattice parameters were investigated. The parameters were obtained by indexing of the observed  $d$  spacings from the patterns shown in Figure 2, using the program CELLKANT.<sup>11</sup> Figure 3a gives the unit cell volume versus temperature. The first decrease (4% relative to the volume of  $\gamma$ -TiP) in the unit cell volume is seen at 69 °C.

(8) Alberti, G.; Cardini-Galli, P.; Costantino, U.; Torracca, E. *J. Inorg. Nucl. Chem.* **1967**, *29*, 571.

(9) Norby, P. *J. Appl. Crystallogr.* **1997**, *30*, 21.

(10) Werner P.-E.; Eriksson, L.; Westdahl, M. *J. Appl. Crystallogr.* **1987**, *18*, 367.

(11) Ersson, N. O. *CELLKANT*; Chemical Institute, Uppsala University: Uppsala, Sweden, 1981.

(12) De Wolff, P. M. *J. Appl. Crystallogr.* **1968**, *1*, 108.

(13) Kobayashi, E.; Yamazaki, S. *Bull. Chem. Soc. Jpn.* **1983**, *56*, 1632.

(14) Llavona, R.; Garcia, J. R.; Suarez, M.; Rodriguez, J. *Thermochim. Acta* **1985**, *86*, 281.

(15) La Ginestra, A.; Massucci, M. A. *Thermochim. Acta* **1979**, *32*, 241.

(16) Pawley, G. S. *J. Appl. Crystallogr.* **1985**, *18*, 367.

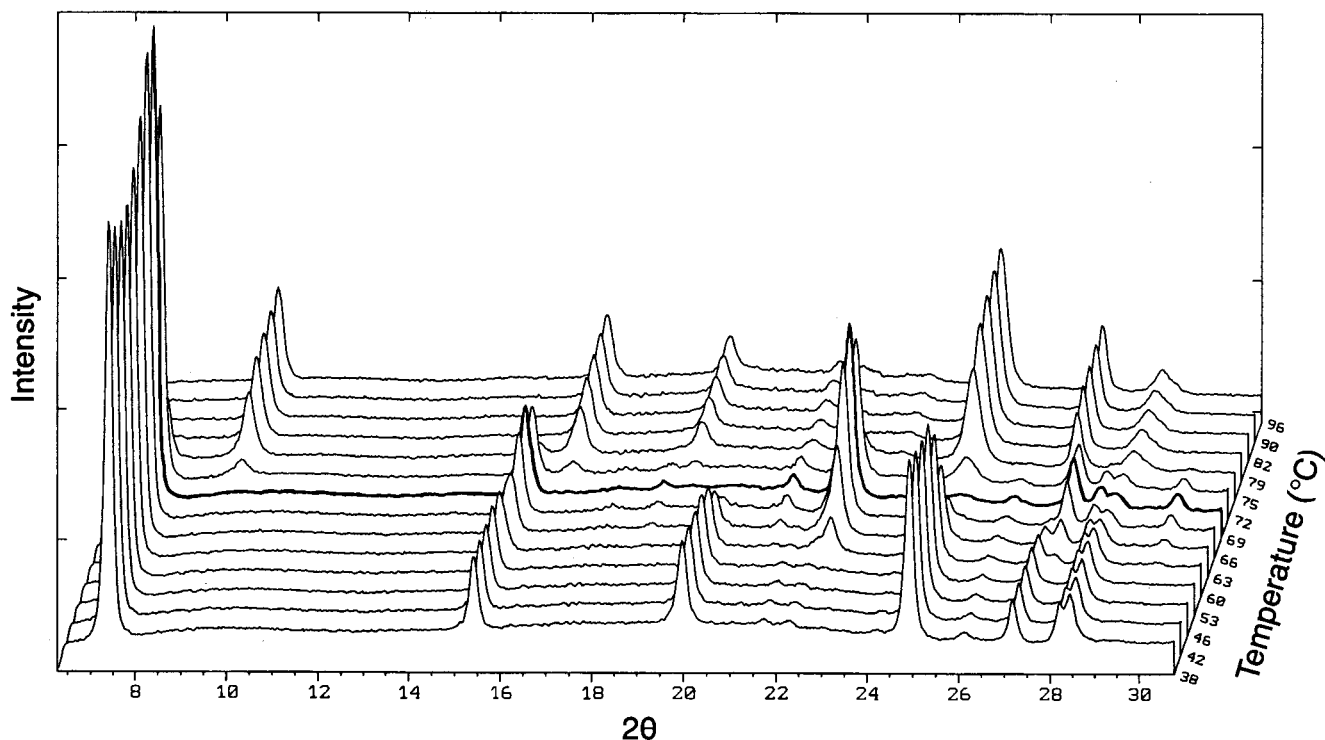


**Figure 2.** Series of synchrotron powder patterns, as a function of temperature, showing the transformation of  $\gamma$ -Ti(PO<sub>4</sub>)(H<sub>2</sub>PO<sub>4</sub>)·2H<sub>2</sub>O to the anhydrous form,  $\beta$ -Ti(PO<sub>4</sub>)(H<sub>2</sub>PO<sub>4</sub>), with the formation of a partially hydrated intermediate,  $\gamma'$ -Ti(PO<sub>4</sub>)(H<sub>2</sub>PO<sub>4</sub>)·(2- $x$ )H<sub>2</sub>O ( $x \sim 1$ ) ( $\gamma'$ -TiP). The pattern of  $\gamma'$ -TiP is highlighted.

**Table 1.** Indexed Powder Pattern of  $\gamma'$ -Ti(PO<sub>4</sub>)(H<sub>2</sub>PO<sub>4</sub>)·(2- $x$ )H<sub>2</sub>O<sup>a</sup>

$h$	$k$	$l$	$d_{\text{calc}}(\text{\AA})$	$d_{\text{obs}}(\text{\AA})$	int	$h$	$k$	$l$	$d_{\text{calc}}(\text{\AA})$	$d_{\text{obs}}(\text{\AA})$	int	$h$	$k$	$l$	$d_{\text{calc}}(\text{\AA})$	$d_{\text{obs}}(\text{\AA})$	int
2	0	0	11.5586	11.5156	100	6	2	0	2.4303	2.4309	1	2	4	0	1.5518	1.5526	1
2	1	0	5.5073	5.5082	3	9	1	0	2.3765	2.3773	1	10	0	2	1.5283	1.5279	1
3	1	0	4.8607	4.8622	1	-6	0	2	2.3102	2.3093	1	3	3	2	1.5175	1.5170	1
-3	0	1	4.6205	4.6177	1	0	1	2	2.2890	2.2884	1	15	1	0	1.4965	1.4961	1
4	1	0	4.2476	4.2484	1	7	2	0	2.2725	2.2710	1	-4	2	3	1.4767	1.4769	1
6	0	0	3.8528	3.8493	7	2	1	2	2.1644	2.1632	1	4	1	3	1.4542	1.4545	1
-5	0	1	3.8009	3.8039	8	-11	0	1	2.1027	2.1023	1	-15	1	2	1.4164	1.4166	1
3	0	1	3.7925	3.7912	8	2	3	0	2.0548	2.0562	1	-17	0	1	1.3896	1.3898	1
-6	0	1	3.4095	3.4121	1	-12	0	1	1.9410	1.9397	1	-13	0	3	1.3597	1.3606	1
6	1	0	3.2818	3.2814	1	-10	0	2	1.9004	1.8989	1	13	3	0	1.3538	1.3526	1
0	2	0	3.1321	3.1314	1	12	1	0	1.8413	1.8421	2	-1	3	3	1.2997	1.2992	1
5	0	1	3.0567	3.0598	2	-13	0	1	1.8006	1.7998	1	8	1	3	1.2824	1.2823	1
8	0	0	2.8896	2.8882	1	8	0	2	1.7010	1.7023	1	2	5	0	1.2455	1.2456	1
8	1	0	2.6239	2.6260	1	14	0	0	1.6512	1.6519	1	-1	1	4	1.2183	1.2185	1
1	2	1	2.5912	2.5902	1	-7	0	3	1.6130	1.6130	1	9	2	3	1.1723	1.1722	1
-1	0	2	2.5025	2.5021	1	14	1	0	1.5967	1.5984	1	-20	1	1	1.1627	1.1627	1
-4	0	2	2.4614	2.4624	1	-6	1	3	1.5873	1.5871	1	7	3	3	1.1377	1.1375	1

<sup>a</sup> The indexing is based on a monoclinic unit cell:  $a = 23.670(3) \text{ \AA}$ ,  $b = 6.264(1) \text{ \AA}$ ,  $c = 5.036(1) \text{ \AA}$ ,  $\beta = 102.41(1)^\circ$ . Data recorded at 54 °C;  $M(20)^{12} = 47.4$ .

This decrease corresponds to the formation of  $\gamma'$ -TiP. The next decrease (18% relative to the volume of  $\gamma'$ -TiP) takes place at 75 °C and corresponds to the conversion of  $\gamma'$ -TiP to  $\beta$ -TiP. The decrease in unit cell volume when  $\gamma'$ -TiP is formed is not due to the slight decrease in interlayer distance (from 11.588 to 11.565 Å), as can be seen from Figure 3b, which shows the lattice parameters versus temperature. From Figure 3b it can clearly be seen that the decrease in unit cell volume at 69 °C is caused by a shortening of the  $b$  and  $c$  axes (by 1.2 and 2.8%, respectively) and not by a decrease in the interlayer parameter ( $a \sin \beta$ )/2. This means that the formation of  $\gamma'$ -TiP is characterized by an intralayer contraction rather than an interlayer rearrangement. When  $\beta$ -TiP forms at 75 °C the interlayer distance is reduced from 11.5 to 9.2 Å. This causes a decrease in the length of the  $a$  axis from 23.670 to 19.104 Å. The length of the  $b$  and  $c$  axis, however, increase and approach the values

found for  $\gamma$ -TiP. So the formation of  $\beta$ -TiP causes a relaxation of the structure of the layers and they approximately return to the structure found in  $\gamma$ -TiP.

**$\beta$ -Titanium Phosphate.** At about 100 °C, 2 mol of crystal water have been lost and the anhydrous form  $\beta$ -TiP is formed. The in-situ synchrotron data obtained at 82 °C have been indexed in a monoclinic unit cell, with lattice parameters  $a = 19.104(4) \text{ \AA}$ ,  $b = 6.315(1) \text{ \AA}$ ,  $c = 5.150(1) \text{ \AA}$ , and  $\beta = 105.45(2)^\circ$ . The indexed pattern is presented in Table 2. These unit cell parameters are in accordance with the room-temperature values for  $\beta$ -TiP found in the structure determination.<sup>7</sup> The unit cell volume is slightly larger due to thermal expansion. The extinctions are in accordance with the space group  $P2_1/n$ , so it can be assumed that there are only minor structural differences between the room-temperature structure and the structure at 82 °C.

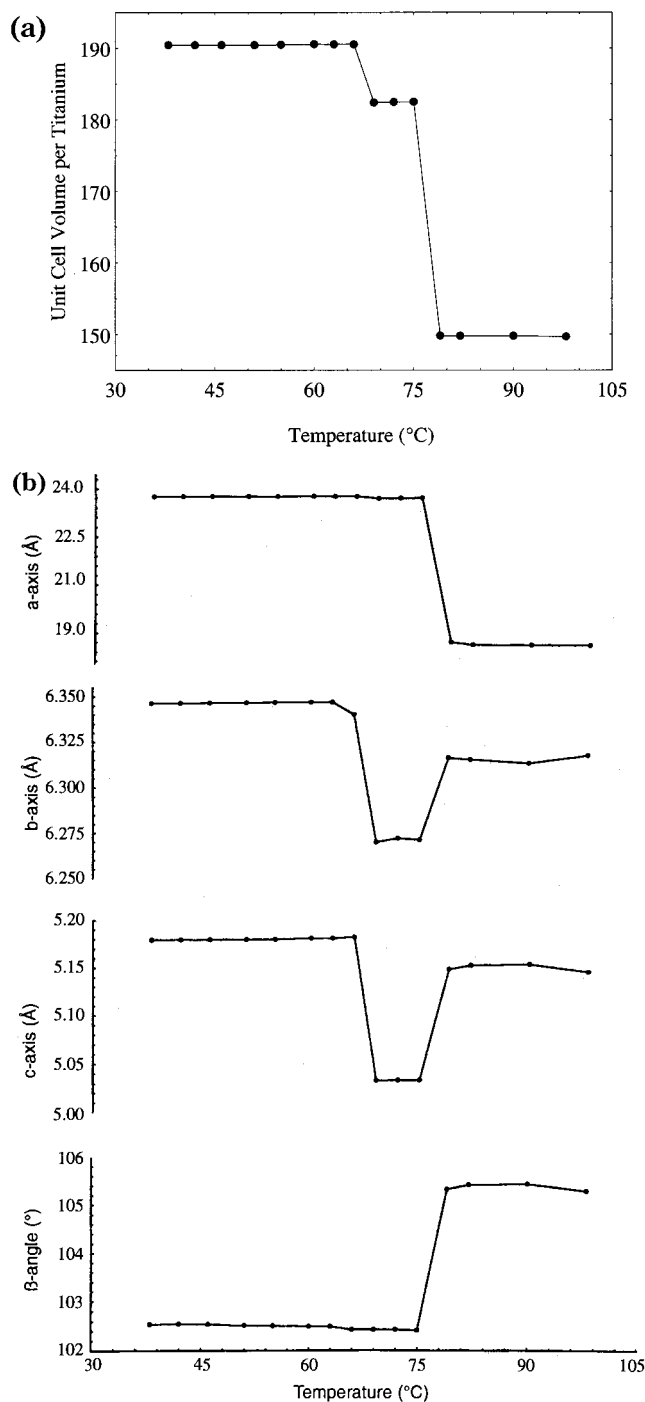


**Figure 3.** Changes in unit cell volume (a) and lattice parameters (b) during the dehydration process from  $\gamma$ -Ti(PO<sub>4</sub>)(H<sub>2</sub>PO<sub>4</sub>)·2H<sub>2</sub>O via  $\gamma'$ -Ti(PO<sub>4</sub>)(H<sub>2</sub>PO<sub>4</sub>)·(2-x)H<sub>2</sub>O ( $x \sim 1$ ) to  $\beta$ -Ti(PO<sub>4</sub>)(H<sub>2</sub>PO<sub>4</sub>).

**Layered Titanium Pyrophosphate.** When the anhydrous material,  $\beta$ -TiP, is heated, hydroxyl condensation takes place. Costantino and La Ginestra<sup>17</sup> propose that this process leads to the formation of layered pyrophosphate. They suggest that the hydroxyl condensation initially leads to the formation of a pyrophosphate phase with a structure similar to that of the starting material, but with adjacent layers joined by P–O–P bridges.

From Figure 4 it can be seen that the hydroxyl condensation of  $\beta$ -titanium phosphate starts at approximately 300 °C. From 300 to 400 °C the compound loses 0.5 mol of water per formula

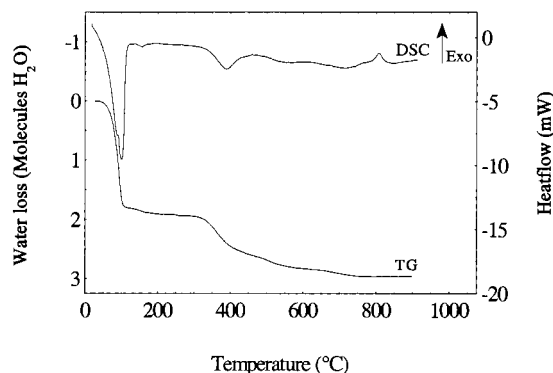


**Figure 4.** TG and DSC curves for  $\gamma$ -Ti(PO<sub>4</sub>)(H<sub>2</sub>PO<sub>4</sub>)·2H<sub>2</sub>O in the temperature range 25–900 °C.

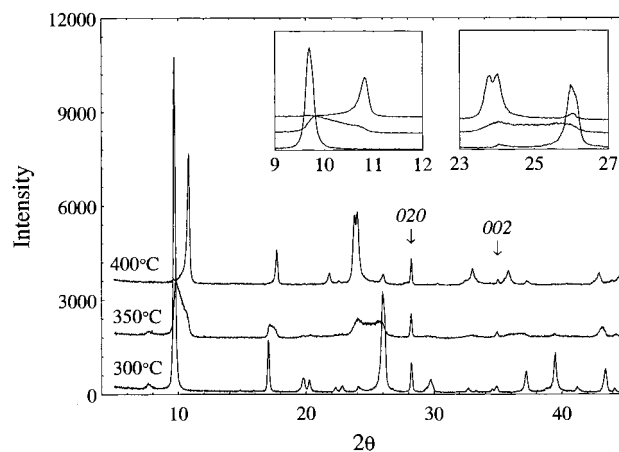


**Figure 5.** X-ray powder patterns of  $\beta$ -TiP ( $\gamma$ -TiP heated to 300 °C), intermediate phase ( $\gamma$ -TiP heated to 350 °C), and layered titanium pyrophosphate ( $\gamma$ -TiP heated to 400 °C). The inserts show selected ranges of the three patterns illustrating the peak-broadening of peaks with a component in the intermediate phase.

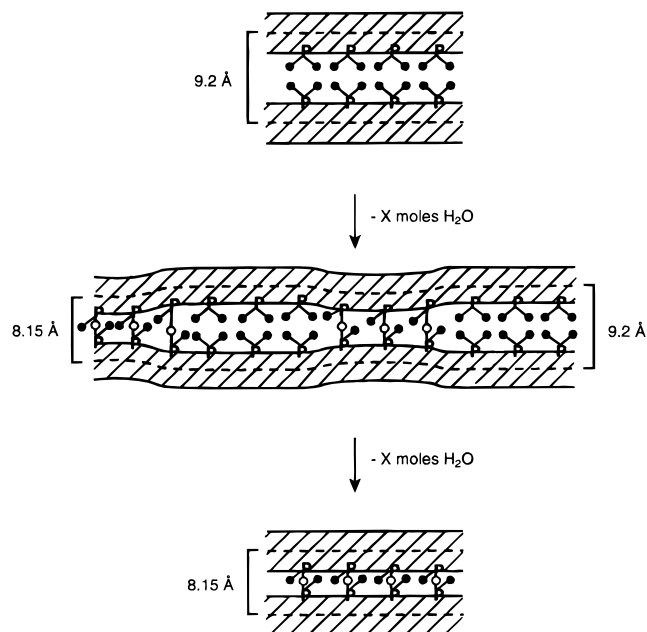


**Figure 6.** Transformation from the anhydrous phase (top) to the layered pyrophosphate (bottom), going through an intermediate phase (middle) with variable interlayer distance due to partial hydroxyl condensation. ● indicates OH groups; ○ indicates oxygen atoms.



**Table 2.** Indexed Powder Pattern for  $\beta$ -Ti(PO<sub>4</sub>)(H<sub>2</sub>PO<sub>4</sub>)<sup>a</sup>

<i>h</i>	<i>k</i>	<i>l</i>	<i>d</i> <sub>calc</sub> (Å)	<i>d</i> <sub>obs</sub> (Å)	int	<i>h</i>	<i>k</i>	<i>l</i>	<i>d</i> <sub>calc</sub> (Å)	<i>d</i> <sub>obs</sub> (Å)	int	<i>h</i>	<i>k</i>	<i>l</i>	<i>d</i> <sub>calc</sub> (Å)	<i>d</i> <sub>obs</sub> (Å)	int
2	0	0	9.2065	9.2636	76	5	1	1	2.4358	2.4350	19	-7	0	3	1.6067	1.6073	15
2	1	0	5.2079	5.2077	64	3	2	1	2.3255	2.3240	17	0	4	0	1.5788	1.5792	12
-3	0	1	4.4883	4.4888	50	-4	2	1	2.3065	2.3074	17	-7	1	3	1.5571	1.5567	12
-1	1	1	3.9911	3.9898	37	7	0	1	2.1039	2.1051	14	-7	3	2	1.4890	1.4890	12
-2	1	1	3.8985	3.9002	35	2	3	0	2.0522	2.0528	16	3	4	1	1.4344	1.4345	13
1	1	1	3.6652	3.6627	30	4	0	2	1.9757	1.9750	17	-2	3	3	1.3272	1.3276	12
3	0	1	3.4376	3.4386	100	-5	3	1	1.7937	1.7936	12	-3	0	4	1.2855	1.2851	12
0	2	0	3.1577	3.1574	58	6	0	2	1.7188	1.7189	12	-15	1	1	1.2482	1.2483	11
3	1	1	3.0193	3.0157	31	-3	1	3	1.6565	1.6571	14	2	5	1	1.2031	1.2029	11
-2	0	2	2.5756	2.5724	26												

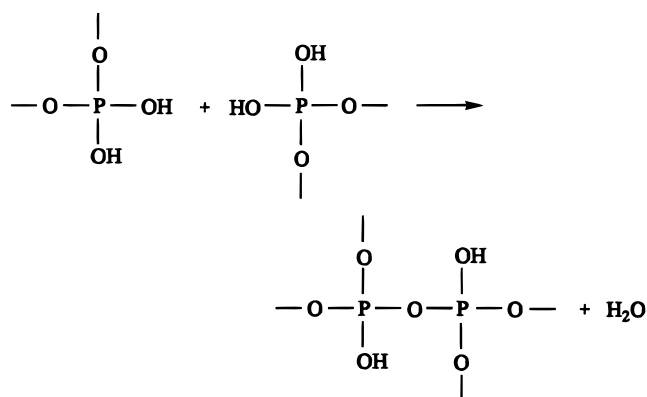
<sup>a</sup> Indexing is based on a monoclinic unit cell:  $a = 19.104(4)$  Å,  $b = 6.315(1)$  Å,  $c = 5.150(1)$  Å, and  $\beta = 105.45(2)^\circ$ . In-situ data recorded at 82 °C;  $M(20)^{12} = 42.6$ .

**Table 3.** Indexed Powder Pattern of Layered Titanium Pyrophosphate Ti(PO<sub>4</sub>)(H<sub>2</sub>P<sub>2</sub>O<sub>7</sub>)<sub>0.5</sub><sup>a</sup>

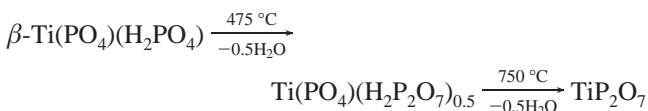
<i>h</i>	<i>k</i>	<i>l</i>	<i>d</i> <sub>calc</sub> (Å)	<i>d</i> <sub>obs</sub> (Å)	int	<i>h</i>	<i>k</i>	<i>l</i>	<i>d</i> <sub>calc</sub> (Å)	<i>d</i> <sub>obs</sub> (Å)	int	<i>h</i>	<i>k</i>	<i>l</i>	<i>d</i> <sub>calc</sub> (Å)	<i>d</i> <sub>obs</sub> (Å)	int
2	0	0	8.1352	8.1912	100	-3	2	1	2.4144	2.4154	4	-8	0	2	1.6006	1.6005	2
2	1	0	4.9906	5.0060	30	-2	1	2	2.2842	2.2854	1	6	3	1	1.5793	1.5795	3
4	0	0	4.0677	4.0775	10	6	1	1	2.2326	2.2333	2	-8	1	2	1.5516	1.5522	3
-3	0	1	3.7428	3.7480	60	-7	0	1	2.1248	2.1234	4	8	1	2	1.5372	1.5362	4
3	0	1	3.7049	3.7120	50	7	0	1	2.1085	2.1086	8	8	3	0	1.4631	1.4628	4
4	1	0	3.4203	3.4272	10	6	2	0	2.0578	2.0582	4	-3	4	1	1.4555	1.4544	2
-3	1	1	3.2204	3.2270	3	2	3	0	2.0392	2.0375	7	-11	1	1	1.3901	1.3897	11
3	1	1	3.1961	3.2015	3	8	1	0	1.9360	1.9359	14	11	1	1	1.3829	1.3830	9
0	2	0	3.1597	3.1636	22	7	2	0	1.8723	1.8734	5	4	4	2	1.2746	1.2749	2
2	2	0	2.9453	2.9494	2	6	0	2	1.8524	1.8521	4	-2	0	4	1.2668	1.2662	2
5	1	0	2.8931	2.8926	2	-6	1	2	1.7944	1.7960	2	-13	0	1	1.2187	1.2182	3
-5	0	1	2.7594	2.7613	4	6	1	2	1.7776	1.7774	2	9	1	3	1.2120	1.2120	3
6	0	0	2.7118	2.7145	14	-9	0	1	1.7102	1.7101	3	-11	3	1	1.1803	1.1798	3
0	0	2	2.5608	2.5641	5	-1	0	3	1.6997	1.6988	2	4	5	1	1.1740	1.1739	3
-5	1	1	2.5288	2.5281	6	5	3	1	1.6686	1.6689	3	-4	2	4	1.1421	1.1422	2
5	1	1	2.5092	2.5093	10	-8	2	1	1.6263	1.6263	9						

<sup>a</sup> The indexing is based on a monoclinic unit cell:  $a = 16.271(3)$  Å,  $b = 6.319(1)$  Å,  $c = 5.122(1)$  Å, and  $\beta = 90.59(2)$ . Room-temperature data;  $M(20)^{12} = 24.1$ .

unit. This corresponds to the condensation of one OH group per dihydrogen phosphate group, giving the formula Ti(PO<sub>4</sub>)-(H<sub>2</sub>P<sub>2</sub>O<sub>7</sub>)<sub>0.5</sub>. This step can be seen schematically as



Between 475 and 750 °C, an additional 0.5 mol of water per formula unit is lost. The conversion to cubic pyrophosphate occurs at 800 °C, indicated by an exothermic peak in the DSC curve. These transitions can be summarized as follows:



Information concerning the structural changes in the first part of the hydroxyl condensation can be obtained by analyzing the powder patterns of  $\gamma$ -TiP heated to 300, 350, and 400 °C shown in Figure 5. At 300 °C the product is the pure anhydrous phase,

*i.e.*  $\beta$ -TiP, and at 400 °C the product is layered titanium pyrophosphate. However, the powder pattern of  $\gamma$ -TiP heated to 350 °C shows the presence of a poorly crystalline phase. The peak broadening is strongly anisotropic. There are a few narrow reflections in the pattern where the assigned indexes have no *a* component. This is the case for the 020 reflection at  $2\theta = 28^\circ$  ( $d = 3.16$  Å) and the 002 reflection at  $2\theta = 35^\circ$  ( $d = 2.56$  Å) in the layered pyrophosphate. The position of these reflections is related to the structure of the layer and not to the interlayer distance. The remaining peaks have indices with an *a* axis component. The anisotropic broadening of the peaks is consistent with variations in the interlayer distance due to the hydroxyl condensation. It can clearly be seen that the peaks with an *a* axis component cover the whole range from  $\beta$ -TiP to the layered pyrophosphate. This is illustrated in the inserts in Figure 5. In fact the 200 reflection in the pattern of the poorly crystalline phase covers *d* values from 9.0 Å (the first *d* value of  $\beta$ -TiP is 9.15 Å) to 8.4 Å (the first *d* value of layered titanium pyrophosphate is 8.18 Å), *i.e.* it covers the whole range in *d* values from the starting compound to the final compound. The conclusion is that the first part of the hydroxyl condensation occurs without or with only slight alterations in the structure of the layer, but with variable layer distance caused by partial hydroxyl condensation. A sketch illustrating this can be seen in Figure 6.

The temperature dependence of the unit cell volume was studied from in-situ temperature-resolved synchrotron powder data. The unit cell volume was obtained by indexing of the observed *d* spacings of a series of patterns in the temperature range 200–850 °C. Figure 7 shows a three-dimensional representation of a small  $2\theta$  range of the diffraction patterns as

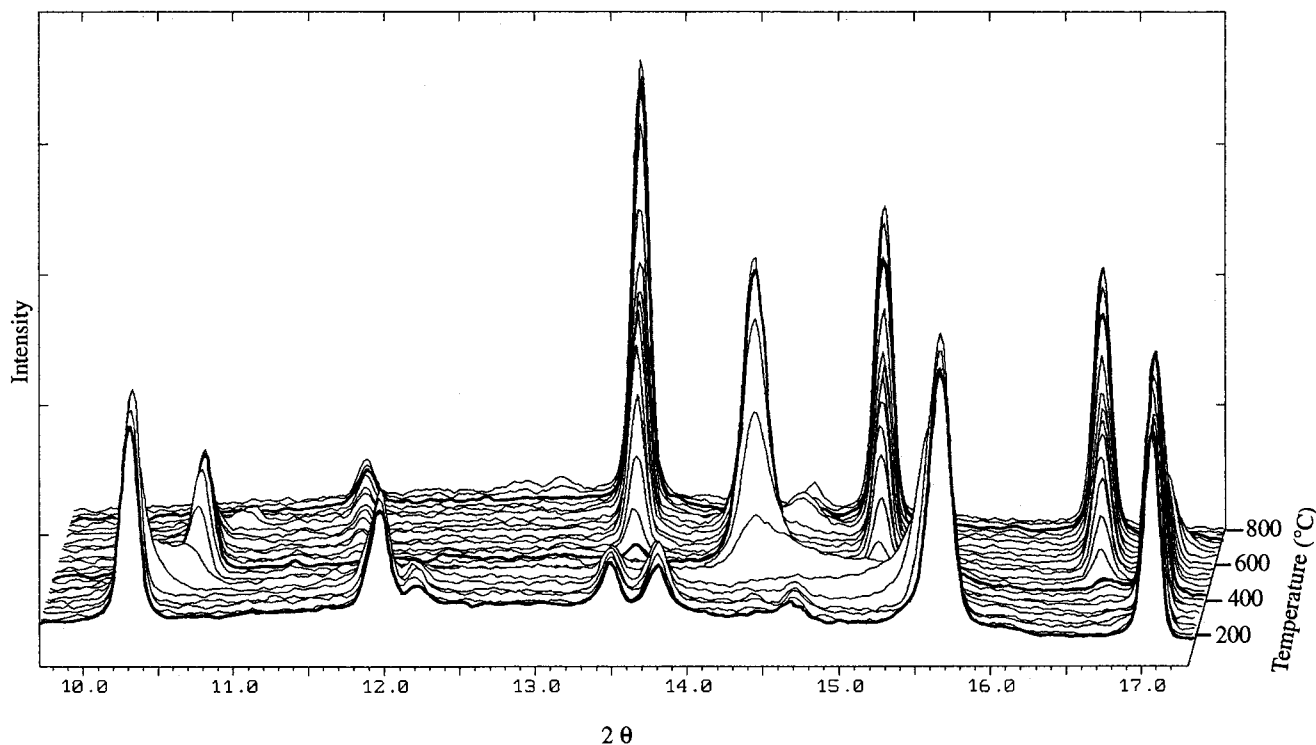


**Figure 7.** Three-dimensional representation of a small  $2\theta$  range of high-temperature powder patterns as a function of temperature in the temperature range 200–800 °C, showing the transformation of anhydrous titanium phosphate ( $\beta$ - $\text{Ti}(\text{PO}_4)(\text{H}_2\text{PO}_4)$ ) via layered titanium pyrophosphate ( $\text{Ti}(\text{PO}_4)(\text{H}_2\text{P}_2\text{O}_7)_{0.5}$ ) to cubic titanium pyrophosphate ( $\text{TiP}_2\text{O}_7$ ). The patterns of the three phases are highlighted.

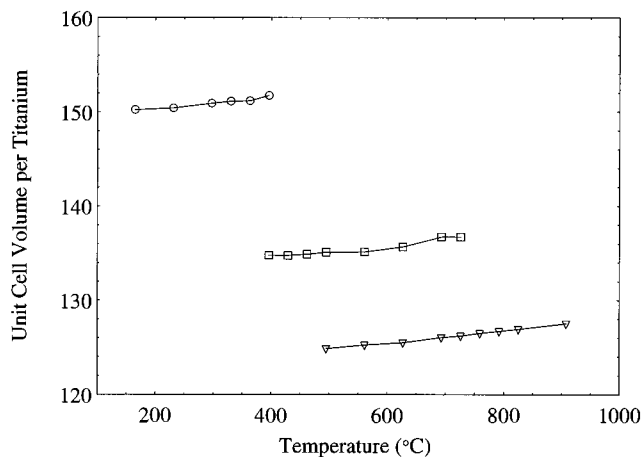


**Figure 8.** Changes in unit cell volume for the transformation of  $\beta$ - $\text{Ti}(\text{PO}_4)(\text{H}_2\text{PO}_4)$  via layered titanium pyrophosphate ( $\text{Ti}(\text{PO}_4)(\text{H}_2\text{P}_2\text{O}_7)_{0.5}$ ) to cubic titanium pyrophosphate ( $\text{TiP}_2\text{O}_7$ ). Circles,  $\beta$ -titanium phosphate; squares, layered titanium pyrophosphate; triangles, cubic titanium pyrophosphate.

a function of temperature. In Figure 8 the unit cell volume versus temperature for  $\beta$ -TiP (circles), layered titanium pyrophosphate (squares), and cubic titanium pyrophosphate (triangles) is shown. First a two-phase system consisting of  $\beta$ -TiP and layered titanium pyrophosphate is present. Shortly after the formation of layered pyrophosphate,  $\beta$ -TiP disappears and a second two-phase system, consisting of coexisting layered titanium pyrophosphate and cubic pyrophosphate, is formed.

As seen in Figure 8 the temperature range of pure layered pyrophosphate is very narrow. It was therefore difficult to obtain a sample of the pure phase. However heating  $\gamma$ -TiP slowly to 375 °C and keeping it at this temperature for 24 h proved to be successful. The indexed powder pattern is provided in Table 3. The unit cell parameters are:  $a = 16.271(3)$  Å,  $b = 6.319(1)$  Å,  $c = 5.122(1)$  Å, and  $\beta = 90.59(2)^\circ$ .

The indexed pattern shows the following systematic extinctions:  $h00$  ( $h = 2n + 1$ ),  $0k0$  ( $k = 2n + 1$ ), and  $h0l$  ( $h + l = 2n + 1$ ) giving  $P2_1/n$  as a possible space group. Profile fitting with GSAS<sup>18</sup> (LeBail) confirms this space group as can be seen in Figure 9.

This part of the hydroxyl condensation is, as mentioned above, connected with a loss of 0.5 mol of water per formula unit. This corresponds to the formation of one P–O–P bridge per dihydrogen phosphate group, giving a compound with the formula  $\text{Ti}(\text{PO}_4)(\text{H}_2\text{P}_2\text{O}_7)_{0.5}$ . The theory about the formation of P–O–P bridges is supported by the presence of several bands in the IR spectra at 1083, 754, 640, and 557  $\text{cm}^{-1}$ . These frequencies are in correspondence with the values reported by Steger *et al.*<sup>19</sup> for  $\text{TiP}_2\text{O}_7$ . These bands are first observed in  $\gamma$ -TiP heated to 350 °C and are present in all the heated samples of  $\gamma$ -TiP up to 1000 °C.

**Cubic Titanium Pyrophosphate.** The final product is cubic titanium pyrophosphate,  $\text{TiP}_2\text{O}_7$ . The exothermic peak in the DSC curve (Figure 4) shows that the cubic phase is formed at 800 °C. In-situ data recorded at 850 °C can be indexed in a cubic cell, with lattice parameter  $a = 7.9899(6)$  Å. The indexed pattern is presented in Table 4a. After cooling to room temperature a  $3 \times 3 \times 3$  superstructure is formed. Room-temperature data have been indexed in a cubic cell, with lattice parameter  $a = 23.6302(5)$  Å. The indexed pattern is provided in Table 4b. The superstructure of titanium pyrophosphate has recently been solved by Sanz *et al.*<sup>20</sup> from X-ray powder diffraction data.

Temperature-resolved in-situ powder diffraction data recorded in the temperature range 200–930 °C were used to study the

(18) Larson, A.; von Dreele, R. B. *GSAS: Generalized Structure Analysis System*; LANSCE, Los Alamos National Laboratory: Los Alamos, NM, 1985.

(19) Steger, E.; Leukrot, G. *Z. Anorg. Allg. Chem.* **1960**, *303*, 169.

(20) Sanz, J.; Iglesias, J. E.; Soria, J.; Losilla, E. R.; Aranda, M. A. G.; Bruque, S. *Chem. Mater.* **1997**, *9*, 996.

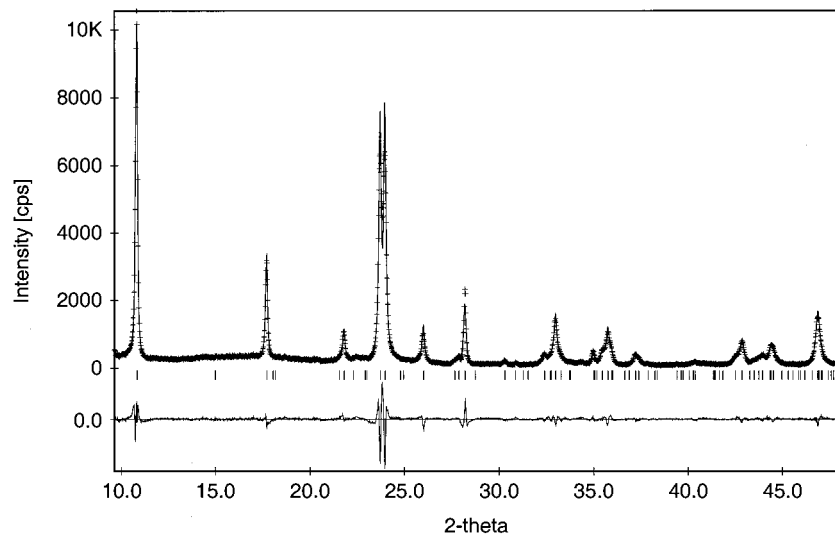


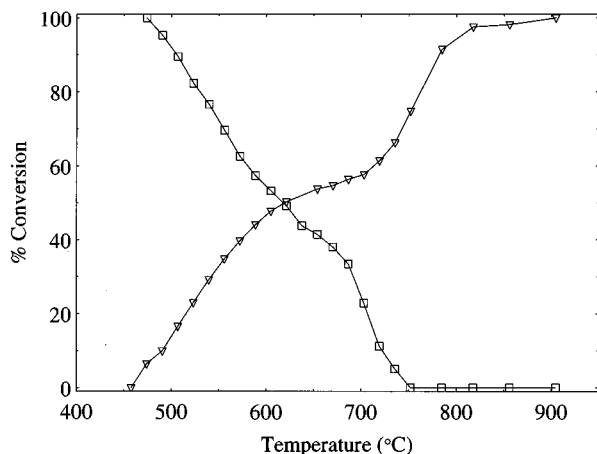
Figure 9. Profile fit (LeBail) for layered titanium pyrophosphate ( $\text{Ti}(\text{PO}_4)(\text{H}_2\text{P}_2\text{O}_7)_{0.5}$ ) in the space group  $P2_1/n$ .

Table 4. Indexed Powder Pattern of Cubic Titanium Pyrophosphate,  $\text{TiP}_2\text{O}_7$

<i>h</i>	<i>k</i>	<i>l</i>	<i>d</i> <sub>calc</sub> (Å)	<i>d</i> <sub>obs</sub> (Å)	int	<i>h</i>	<i>k</i>	<i>l</i>	<i>d</i> <sub>calc</sub> (Å)	<i>d</i> <sub>obs</sub> (Å)	int	<i>h</i>	<i>k</i>	<i>l</i>	<i>d</i> <sub>calc</sub> (Å)	<i>d</i> <sub>obs</sub> (Å)	int	
(a) In-Situ Data Recorded at 850 °C; Indexing Based on Cubic Unit Cell, Lattice Parameter $a = 7.9899(6)$ Å; $M(20)^{12} = 54.4$																		
1	1	1	4.6130	4.6163	23	3	3	1	1.8330	1.8339	6	4	4	2	1.3317	1.3316	6	
2	0	0	3.9950	3.9938	100	4	2	0	1.7866	1.7866	13	5	3	2	1.2961	1.2960	6	
2	1	0	3.5732	3.5732	71	4	2	1	1.7435	1.7431	8	6	2	0	1.2633	1.2632	4	
2	1	1	3.2619	3.2650	61	3	3	2	1.7035	1.7020	5	5	4	1	1.2329	1.2320	3	
2	2	0	2.8249	2.8262	18	4	2	2	1.6309	1.6314	11	5	3	3	1.2184	1.2180	4	
3	1	1	2.4091	2.4104	19	4	3	0	1.5980	1.5995	5	5	4	2	1.1911	1.1910	4	
2	2	2	2.3065	2.3078	7	3	3	3	1.5377	1.5378	14	6	3	1	1.1780	1.1780	4	
3	2	0	2.2160	2.2157	11	4	3	2	1.4837	1.4842	5	5	4	3	1.1299	1.1304	3	
3	2	1	2.1354	2.1365	8	5	2	1	1.4588	1.4592	6	6	4	0	1.1080	1.1079	3	
4	0	0	1.9975	1.9994	8	4	4	0	1.4124	1.4124	8	5	5	2	1.0873	1.0868	2	
3	2	2	1.9378	1.9380	11	5	3	1	1.3505	1.3495	4	5	4	4	1.0583	1.0587	3	
3	3	0	1.8832	1.8827	8													
(b) Room-Temperature Data; Indexing Based on Cubic Unit Cell, Lattice Parameter $a = 23.6302(5)$ Å; $M(20)^{12} = 100.0$																		
2	0	0	11.8147	11.7933	2	8	7	3	2.1394	2.1391	1	13	6	3	1.6153	1.6154	2	
3	3	3	4.5476	4.5460	2	7	7	5	2.1307	2.1295	1	10	10	4	1.6078	1.6078	2	
4	4	2	3.9384	3.9371	100	8	6	5	2.1135	2.1137	1	11	7	7	1.5968	1.5971	1	
6	1	0	3.8848	3.8857	2	9	6	3	2.1051	2.1047	1	11	8	6	1.5895	1.5897	1	
5	3	2	3.8333	3.8317	1	9	5	5	2.0646	2.0645	2	10	10	5	1.5753	1.5753	1	
6	2	0	3.7363	3.7369	2	7	7	6	2.0411	2.0411	1	12	7	6	1.5615	1.5614	1	
5	3	3	3.6036	3.6028	1	9	7	3	2.0043	2.0046	2	10	9	7	1.5581	1.5580	1	
5	4	2	3.5226	3.5221	22	8	8	4	1.9692	1.9689	1	14	6	0	1.5514	1.5514	1	
6	3	2	3.3757	3.3758	2	9	7	4	1.9556	1.9560	1	12	8	6	1.5481	1.5474	1	
5	5	2	3.2157	3.2154	12	12	2	0	1.9424	1.9414	1	10	10	6	1.5382	1.5393	1	
5	5	3	3.0764	3.0760	1	8	7	6	1.9359	1.9358	1	11	9	6	1.5317	1.5318	2	
6	4	3	3.0255	3.0253	1	10	5	5	1.9294	1.9281	1	9	9	9	1.5159	1.5160	7	
7	3	2	3.0010	2.9996	1	8	8	5	1.9104	1.9101	4	12	10	2	1.5005	1.5001	1	
6	4	4	2.8656	2.8659	2	9	7	5	1.8980	1.8975	1	12	9	5	1.4945	1.4943	2	
6	6	0	2.7848	2.7848	2	11	6	0	1.8859	1.8856	1	13	7	6	1.4827	1.4821	1	
8	3	0	2.7657	2.7645	1	12	4	0	1.8681	1.8682	1	11	10	6	1.4740	1.4740	1	
7	4	3	2.7470	2.7470	1	8	7	7	1.8566	1.8566	3	12	9	6	1.4627	1.4625	1	
6	5	4	2.6929	2.6928	1	8	8	6	1.8452	1.8451	1	12	11	0	1.4516	1.4514	1	
8	4	0	2.6419	2.6424	2	9	7	6	1.8341	1.8331	1	11	10	7	1.4381	1.4379	2	
8	3	3	2.6095	2.6101	1	12	4	3	1.8177	1.8178	1	13	9	5	1.4250	1.4247	1	
7	5	3	2.5937	2.5929	1	9	9	3	1.8070	1.8069	1	14	9	0	1.4198	1.4190	1	
6	5	5	2.5481	2.5489	1	10	8	3	1.7966	1.7962	1	10	10	9	1.4097	1.4098	1	
7	6	2	2.5048	2.5041	1	9	9	4	1.7712	1.7712	1	13	9	6	1.3973	1.3980	1	
7	6	3	2.4373	2.4373	1	10	8	4	1.7613	1.7613	3	12	12	0	1.3924	1.3923	2	
7	5	5	2.3749	2.3750	6	10	7	6	1.7373	1.7381	1	13	10	5	1.3781	1.3780	1	
8	6	0	2.3630	2.3631	3	9	9	5	1.7280	1.7278	1	12	12	3	1.3712	1.3715	1	
7	6	4	2.3513	2.3507	2	10	8	5	1.7188	1.7188	2	13	9	7	1.3666	1.3665	1	
8	6	2	2.3171	2.3166	2	9	8	7	1.6965	1.6967	1	17	3	3	1.3486	1.3484	1	
9	4	3	2.2952	2.2943	1	12	6	4	1.6879	1.6879	1	12	11	7	1.3335	1.3345	1	
7	7	3	2.2844	2.2845	1	9	9	6	1.6793	1.6789	1	13	11	5	1.3314	1.3315	1	
6	6	6	2.2738	2.2743	2	10	8	6	1.6707	1.6707	2	13	12	2	1.3272	1.3269	1	
8	6	3	2.2634	2.2621	1	13	5	3	1.6585	1.6588	1	12	12	6	1.3128	1.3125	1	
7	6	5	2.2530	2.2524	1	12	6	5	1.6504	1.6502	1	16	6	6	1.3048	1.3043	1	
8	7	0	2.2229	2.2230	1	10	9	5	1.6464	1.6466	1	13	10	8	1.2949	1.2949	1	
8	7	2	2.1846	2.1847	3	9	8	8	1.6345	1.6344	1	12	12	7	1.2872	1.2872	1	
7	6	6	2.1482	2.1477	1	12	8	2	1.6229	1.6228	2	11	11	10	1.2778	1.2778	2	

transformation from layered titanium pyrophosphate to cubic titanium phosphate. Figure 7 shows a 3-dimensional represen-

tation of a small  $2\theta$ -range of the patterns as a function of temperature. At 450 °C only the strongest peaks of cubic



**Figure 10.** Transformation curves for the conversion of layered titanium pyrophosphate (squares) to cubic titanium pyrophosphate (triangles).

pyrophosphate are visible in the powder patterns. However, the peaks of cubic pyrophosphate get more and more dominant when the temperature is raised, as can be seen in Figure 7, until at 750 °C the pure phase is obtained. A few extra lines (e.g. at  $2\theta = 11.3$  and  $14.7$ ) appear before the formation of cubic pyrophosphate. This could indicate the existence of an intermediate phase. Figure 10 shows the transformation curves for the conversion of layered pyrophosphate to cubic pyrophosphate. The progress of the transformation was estimated from integrated intensities of diffraction lines. Well-resolved diffraction lines with no overlap between the two phases were used: for layered pyrophosphate the 200, 210, and  $\bar{3}01$  reflections, and

for cubic pyrophosphate the 200, 210, and 211 reflections. The integrated intensities of the selected reflections were added and normalized to represent the percentage of the phase present. Figure 10 shows the normalized integrated intensities of diffraction lines of layered pyrophosphate and cubic pyrophosphate plotted as a function of temperature. The curves cross close to 50% conversion. This implies that there is no significant amount of amorphous material involved in the transformation. If there had been significant amounts of amorphous material present the conversion curves would have crossed below 50%.

### Conclusion

The thermal transformations of  $\gamma$ -titanium phosphate to cubic titanium pyrophosphate proceed via a number of intermediate phases. The dehydration of  $\gamma$ - $\text{Ti}(\text{PO}_4)(\text{H}_2\text{PO}_4)\cdot 2\text{H}_2\text{O}$  takes place in two steps. First a partially dehydrated intermediate phase  $\gamma'$ - $\text{Ti}(\text{PO}_4)(\text{H}_2\text{PO}_4)\cdot(2-x)\text{H}_2\text{O}$  ( $x \sim 1$ ) is formed and then the anhydrous phase  $\beta$ - $\text{Ti}(\text{PO}_4)(\text{H}_2\text{PO}_4)$  forms. The dehydroxylation/condensation processes also take place in two steps with the formation of layered titanium pyrophosphate,  $\text{Ti}(\text{PO}_4)(\text{H}_2\text{P}_2\text{O}_7)_{0.5}$ , and then the final product cubic titanium pyrophosphate,  $\text{TiP}_2\text{O}_7$ . All the phases in the transformation sequence have been indexed.

**Acknowledgment.** The authors thank Jonathan C. Hanson (Brookhaven National Laboratory) and Torben R. Jensen (University of Odense) for their collaboration.

IC9801894